Modelling Effect of Rain on Aerodynamic Performance of the Ahmed Body

Parth Y. Patel[1], Jia-Hua Liu[2], Vladimir V. Vantsevich[3], Roy Koomullil[4]

University of Alabama at Birmingham, Birmingham, Alabama, 35294, USA

Flow around the Ahmed body is a well-recognized benchmark test case used by the computational fluid dynamics (CFD) community for model validation of automobiles. Even though the geometry of the Ahmed body is simple, the flow field around the object is complex due to flow separation and vortex shedding. In this paper, a Discrete Phase Model (DPM) based computational methodology is presented to estimate the effect of rain on aerodynamic performance and is validated with the experimental data that is available in the literature for the NACA64-210 wing section under different rain intensities. With this validated model, we have investigated the Ahmed body under low and high rain intensities for base slant angles of 25^o and 35^o. The computed drag coefficient for the Ahmed body under rain conditions, are compared with the experimental data from aerodynamic analysis of the Ahmed body without rain, to evaluate the rain effect.

Keywords: The Ahmed Body, Rain Modelling, Discrete Phase Model (DPM), Automotive Aerodynamics, NACA64-210 Airfoil

I. Introduction

The freight, and utility transportation systems are the dominant methods of moving commerce, providing services, and saving lives, nationally and internationally. Moreover, the truck fleets "rule" the strain on the environment, resource consumption, and amplify citizen's exasperation. There were approximately 2.83 million truck drivers in the country in 2014, 28.2% of drivers drove various service trucks [1]. Utility trucks (also known as boom trucks) are the first responders in extreme climate and weather situations for saving people's lives, for restoring electric power, cutting trees, and restoring traffic on roads. When high-speed vehicles are running under heavy rain and crosswind conditions, the aerodynamic forces and moments may increase significantly, resulting in the instability of the vehicle. These weather conditions also hinder the driver's visibility and reduces the tire-road friction force, and further, it influences the driving safety. The adverse weather always puts the drivers and the vehicles in critical hazardous conditions and increases the risk of accidents. Thus, it is extremely necessary to control the aerodynamic forces and moments of the vehicle under severe weather conditions. Even though the aerodynamic forces are critical in the vehicle stability under severe weather conditions, there is not much information available in the literature addressing this issue. Many previous studies have analyzed the aerodynamic performance of the wing in heavy rain conditions [2]-[5].

The heavy rain has created a critical cause in the aerodynamic performance of the aircrafts, resulting in the severe aviation accidents [6]. There have been three methods to study the aerodynamic performance of aircrafts, and wings under rain conditions, i.e., wind tunnel experiments, numerical experiments, and flight tests. On the experimental side, the effect of heavy rain on an aircraft was reported by Rhode [2] in 1941. He performed the wind tunnel test of DC-3 aircraft flying through a rainstorm with Liquid Water Content (LWC) of 50 g/m^3. Hansman and Craig [7] conducted a wind tunnel experiments on a Wortman FX67-K170, NACA64-210 airfoil in simulated rain rate of 1000 mm/hr and Reynolds number of 310,000 to compare the aerodynamic performance degradation of the airfoil in heavy rain conditions. Bezos and Campbell [5] developed a large-scale, outdoor, ground-based test capability to acquire the aerodynamic data in a simulated rain environment to assess the effect of rain on airfoil performance. Bezos and Gaudy

[8] performed the wind tunnel aerodynamic characteristics of a transport type airfoil in a simulated heavy rain environment. The intent of the investigation was (i) to determine the effect of rain severity on a cambered airfoil representative of typical commercial transport wing sections, (ii) to determine the aerodynamic penalty over a broader range of rain intensities, and (iii) to explore the importance of surface tension interactions of water as a scaling parameter.

As computational fluid dynamics (CFD) developed around the early 1990s, several researchers simulated airfoils and wings' aerodynamic performance using a numerical simulation approach. Benyin Lv and Zhenlong Wu [3] have conducted numerical simulations on the DHC-6 Twin Otter wing and horizontal tail plane to explore the aerodynamic penalties that affect airfoil performance in heavy rain conditions. Yihua Cao and Zhenlong Wu [6] analyzed the aerodynamics of the aircraft under the impact of heavy rainfall. There have been several studies [4][8] that simulated heavy rain conditions and characterized the aerodynamic performance of a NACA 64-210 wing section. Ismail and Yihua [9] have conducted numerical simulations of the heavy rain effects on the aerodynamic efficiency of cambered NACA 64-210 and symmetric NACA 0012 airfoils. Shao and Wan [10] investigated the impact of heavy rainfall on train aerodynamics coupling with heavy rain and strong crosswind. Their results show that the side force, lift force, and rolling moment of the train increases significantly with wind speed of up to 40 m/s under rainfall rate of 60 mm/h.

There are very few publications [10][11] that discuss about the aerodynamic performance of vehicles like cars/trucks under heavy rain conditions. Rahman and Lownes [12] studied the impact of rainfall on drivers' behavior by analyzing the differences in time gap, speed, and following distance of platooned vehicles between no-rain and rainy weather conditions. They utilized the rain intensity as the measure of local precipitation conditions. Billot et al. [13] and Saberi and Bertini [14] consider different levels of rain intensity on the maximum speed and its effect on driving behavior. Harada and Kitamura [11] developed a simplified, one-way coupled, Discrete Droplet Method to model multiple rain-droplet motions over the vehicle wall. However, there is not much information available in the literature on the effect of rain on the aerodynamic performance of automobiles.

The automobile geometry such as the utility truck is very complex to model and study experimentally in real life. However, the geometry of the Ahmed body represented in figure 1, proposed by Ahmed et al. [15] features real vehicle flow field characteristics in three dimensions. The Ahmed body is a well-accepted benchmark case for both academic and industrial applications due to its geometric simplicity, while maintaining vehicle flow features. The geometry has a length of 1.044 meters with the ratio of the length, width, and height being 3.36: 1.37: 1. The middle of the body is a cuboid, and the edges of the front body are curved. There is a slant surface at the top rear whose angles range between 0^o and 40^o degrees. It also has four-cylindrical poles called stilts, attached to the bottom of the main body. The Ahmed body geometry has been used in many aerodynamic experiments in the previous studies [15][16]. Many of these studies have investigated two specific slant angles, 25^o and 35^o, on the Ahmed body's rear top surface, as represented in figure 2, to visualize the flow around the Ahmed body. The airflow is separated evenly when the rear top slant angle is at 30^o and is called critical slant angle at which the drag is maximum. The rear slant angle 25^o corresponds to the high drag configuration which exhibits strongly three-dimensional wake. In contrast, the 35^o rear slant angle is the low drag configuration which exhibits quasi two-dimensional wake.

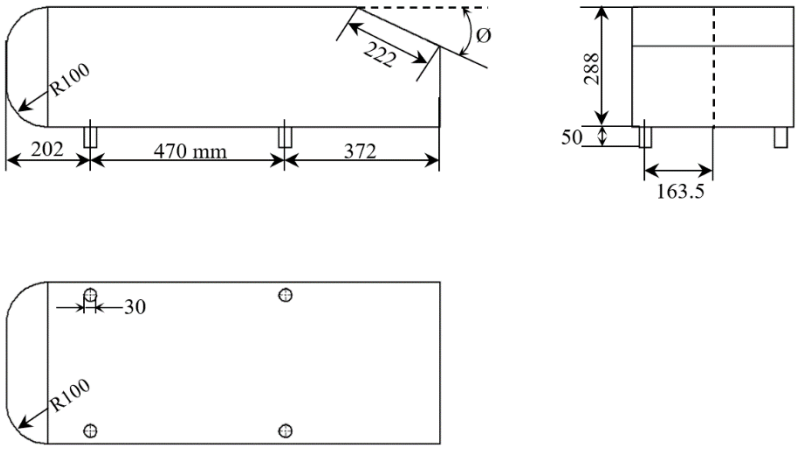

Figure 1. Geometry of Ahmed Body

a) b)

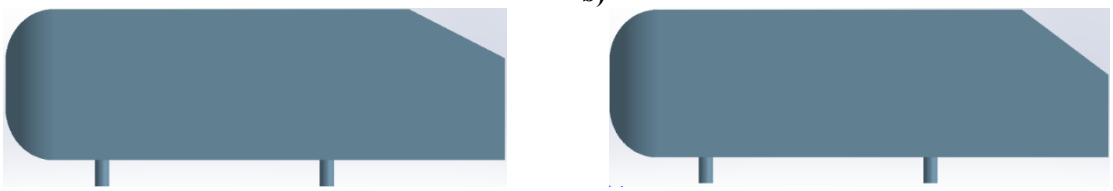

Figure 1.2. Ahmed body (a) 25° rear slant angle (b) 35° rear slant angle

This paper presents a DPM based numerical method to evaluate the effect of rain on aerodynamic performance of objects. The presented model is validated with the experimental data available for a NACA64-210 wing section and the numerical results are compared with the experimental data and the numerical results published in the literature. The validated model is used to numerically investigate the flow around the Ahmed body. Details of the modelling of rain particles, numerical modelling using incompressible unsteady Reynolds Averaged Navier Stokes (URANS) equations, and multi-phase flows, and the results from the numerical studies are discussed in the following sections.

II. Modelling of Rain Particles

In the experimental or numerical simulation, the rainfall intensities are commonly specified in terms of Liquid Water Content (LWC) in the air. The relation between rainfall rate R (mm/h) to LWC (g/m^3) for the thunderstorm type rain is given by the relation [8]

$$LWC = 0.054R^{0.84} \tag{1}$$

and for light spread type rain, it is given by

$$LWC = 0.0889R^{0.84} \tag{2}$$

Typical values of LWC for medium intensity rain is 19 gm/m^3 and heavy rain is 30 gm/m^3. Another parameter that is important in the simulation of objects under rain condition is the terminal velocity. This influences the momentum that is imparted on the body during the impingement of rain droplets on the object. As the rain droplets falls through the atmosphere, it accelerates and as the velocity increases the drag force acting on the droplets also increases. At the terminal velocity, the gravitational force balances with the drag force and the raindrops stop accelerating. Markowitz [21] presented an equation to estimate the terminal velocity as a function of the diameter of the rain droplets as

$$V_T\left(\frac{m}{s}\right) = 9.58\left\{1 - exp\left[-\left(\frac{d(mm)}{1.77}\right)^{1.147}\right]\right\} \tag{3}$$

where, V_T is the terminal velocity in (m/sec), and d is the rain droplet size in mm.

III. Numerical Modelling

The flow features around bluff bodies are typically unsteady in nature due to flow separation and vortex shedding, even for a steady incoming flow. Therefore, it advisable to conduct the simulation in an unsteady mode and take a time average value of the parameters of interest from the simulation. One of the approaches for resolving the small-scale turbulent fluctuations in an unsteady flow field is the large eddy simulations (LES). However, this could be computationally expensive. Alternatively, the unsteady Reynolds averaged Navier Stokes (URANS) simulation is frequently used in the investigation of long-term periodical oscillations in a turbulent flow and this approach is adopted to conduct the simulations presented in this paper.

With the usual notations, the incompressible unsteady Reynolds Averaged Navier Stokes (URANS) equations is written as [22]

$$\frac{\partial \rho}{\partial t} + \frac{\partial(\rho u_i)}{\partial x_i} = 0 \tag{4}$$

$$\frac{\partial(\rho u_i)}{\partial t} + \frac{\partial(\rho u_i u_j)}{\partial x_j} = -\frac{\partial p}{\partial x_i} + \frac{\partial}{\partial x_j}\left[\mu\left(\frac{\partial u_i}{\partial x_j} + \frac{\partial u_j}{\partial x_i} - \frac{2}{3}\delta_{ij}\frac{\partial u_l}{\partial x_l}\right)\right] + \frac{\partial}{\partial x_j}\left(-\rho\overline{u_i' u_j'}\right) \quad (5)$$

The Reynolds stress appearing in the momentum equation can be written using the Boussinesq hypothesis as [22]

$$-\rho\overline{u_i' u_j'} = \mu_t\left(\frac{\partial u_i}{\partial x_j} + \frac{\partial u_j}{\partial x_i}\right) - \frac{2}{3}\left(\rho k + \mu_t\frac{\partial u_k}{\partial x_k}\right)\delta_{ij} \quad (6)$$

The eddy viscosity μ_t in the above equation is estimated using the two equations $k-\omega$ shear-stress transport (SST) turbulence model. The advantage of using this turbulence model is that it considers the transport of the principal turbulence shear stress in the near wall region. The pressure-based flow solver available in ANSYS is used for the solution of the governing equations, which utilizes a finite volume method to discretize them. There are two pressure-based algorithms available in the ANSYS Fluent (i) a segregated algorithm, and (ii) a coupled algorithm [22]. In the segregated algorithm, each component of the governing equation is solved sequentially, and an iterative approach is used to achieve convergence at every time step. The segregated approach is memory efficient. However, the convergence rate is relatively slow in lieu of the equations are solved in a decoupled manner. The Coupled algorithm solves a coupled system of equations comprising the continuity equation and the momentum equations simultaneously. The convergence rate can be significantly improved in the coupled approach as compared to the segregated approach. In both these approaches, the turbulence model equations for the solution variable are solved one after another using a segregated algorithm.

IV. Multi-Phase Flow Approach

Currently, there are two main approaches available for the numerical calculation of the multi-phase flows: the Eulerian-Eulerian approach and the Eulerian-Lagrangian approach. In the Eulerian-Eulerian approach, the different phases are treated mathematically as separate continuous mediums. The concept of phase volume is introduced in this approach since the volume occupied by one phase cannot be occupied by another phases. An assumption is made for the volume fractions to be continuous in space and time, and their sum is equal to one. In this approach, the fluid phases are treated as continuum by solving the unsteady Reynolds Averaged Navier Stokes equations. In the Eulerian-Lagrangian approach, the under laying continuous medium is solved using the Eulerian approach and the dispersed phase is solved by tracking a large number of particles, bubbles, or droplets using a Lagrangian approach in the continuous medium. During these trajectory calculations, it is assumed that the dispersed phase can exchange momentum with the continuous phase. Additionally, we can simulate a discrete second phase consisting of spherical particles in a Lagrangian reference frame, and this model is called Discrete Phase Model (DPM). In order to simulate the rain environment, the DPM is employed in this paper.

ANSYS Fluent [22] provides the capability to predict the trajectory of rain droplets by integrating the force balance on the particle, which is written in a Lagrangian reference frame. This balance of forces acting on the particle can be written as

$$\frac{d\vec{u}_p}{dt} = F_D\left(\vec{u} - \vec{u}_p\right) + \frac{\vec{g}\,(\rho_p - \rho)}{\rho_p} + \vec{F} \quad (7)$$

where $\vec{F}$ is an additional acceleration (force/unit particle mass), $F_D\left(\vec{u} - \vec{u}_p\right)$ is the drag force per unit particle mass, $\vec{u}$ is the fluid phase velocity, $\vec{u}_p$ is the particle velocity, ρ is the fluid density, ρ_p is the density of the particle, and F_D is defined as:

$$F_D = \frac{18\,\mu\,C_d\,Re}{\rho_p d_p^2\,24} \quad (8)$$

where, μ is the molecular viscosity of the fluid, C_d is drag coefficient, ρ is the fluid density, ρ_p is the density of the particle, d_p is the particle diameter, and Re is the relative Reynolds number, which is defined as

$$Re \equiv \frac{\rho d_p|\vec{u}_p - \vec{u}|}{\mu} \quad (9)$$

One of the parameters needed by ANSYS Fluent for DPM simulations is the mass flow rate of the DPM phase. In the following simulations, the DPM mass flow rates are specified at the inlet. To calculate the mass flow rate of the DPM phase, the volume flow rate is calculated using the product of the inlet area and the inlet velocity, and the resulting volume flow rate is multiplied by the rain intensity (LWC). For example, for an injection area of 30m×1m and the free stream velocity is 40 m/s, the volume flow rate is 1200 m^3/s. For a medium rain intensity (LWC) of 19 g/m^3 the mass flow rate for DPM is 22.8 kg/s. Another parameter that is needed for DPM simulation is the size distribution of the dispersed medium. Based on the data available from the literature [23][24], the minimum, maximum, and mean diameter of the droplets are defined as 0.5 mm, 2.5 mm, and 1.5 mm, respectively. Finally, the two-way coupling between the continuous phase and discrete phase is used to simulate more accurate rain behavior.

V. Numerical Results

One of the important steps in the computational simulations is the estimation of the accuracy of the computational results using theoretical or benchmark experimental data. For aerodynamics applications, the approach to achieve this verification is by comprising the lift and drag coefficients and velocity profiles with the experimental data and numerical results. In this study, the computational modeling methodology for Discrete Phase Model (DPM) is validated using the experimental data available for the NACA64-210 wing section [4][25]. The numerical models for the simulation of continuous medium is validated using the computed drag coefficient and velocity profiles for the air flow around the Ahmed body without rain and the available experimental data [15][26]. These validated models for the DPM and continuous medium are used for the analysis of aerodynamic performance of the Ahmed body under rain conditions, for which no experimental or simulation data is available in the literature.

A. Validation of the DPM Model

NACA64-210 airfoil profile is one of the commonly used profiles for wings for many modern transport aircrafts. Aerodynamic performance data for this NACA64-210 is available in Theory of Wing Sections [25]. Experimental data is also available for this airfoil in the literature from the measurements of lift and drag coefficient for different rain conditions [5][8]. Researchers has used this data for the validation of numerical simulations of rain models and the comparisons are also available in the literature [4,7,9]. Therefore, we have selected this as the benchmark testcase for the validation of the DPM model used in our simulations. The wing section for this testcase has a chord length of 3.048m. We have used a quad-dominant mesh for the discretization of the wing cross-section and an extruded mesh is used for the discretization of the three-dimensional computational domain. A view of the mesh on one of the ends of the wing section is shown in figure 5.1. The three-dimensional mesh consists of 388345 elements and 473952 nodes.

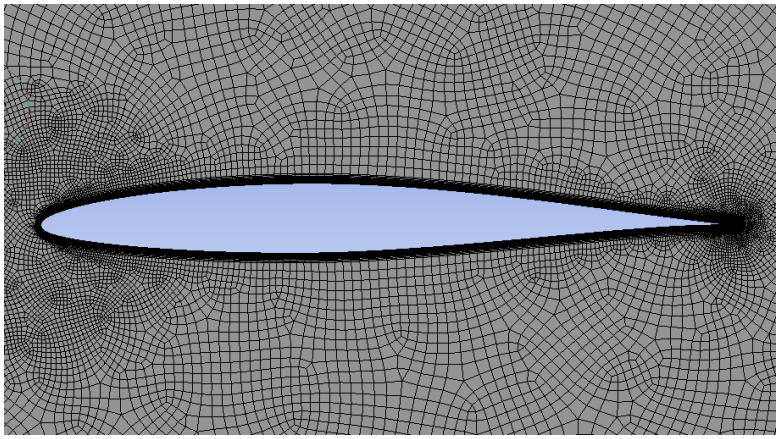

Figure 5.1. Near mesh of NACA64-210 airfoil

Based on the experimental data, the inlet velocity for the simulation is taken as 62.517 m/s. For the DPM model, a reflect boundary condition with the polynomial of normal and tangential discrete phase reflection coefficients is specified at the wing surface [22]. The normal coefficient defines the amount of momentum in the direction normal to the wall that is retained by the particle after the collision with the boundary. Similarly, the tangential coefficient defines the amount of momentum in the direction tangential to the wall that is retained by the particle. Simulations are conducted with two different rain intensities, LWC of 19 g/m^3 and 30 g/m^3, and the various angles of attack, to investigate the rain effects on the wing. Ansys Fluent does not take the force exerted by the DPM particles in the calculation of drag and lift coefficients using the built-in report definition functions. However, it reports the components of the forces exerted by DPM particles in each coordinate directions. These force components are used for the estimation of drag and lift coefficients due to DPM particle impingement and are added to the corresponding coefficients to get the total force coefficients. Figure 5.2 shows the comparison between drag and lift coefficients from different numerical simulations with the experimental data. It can be seen from the figure that there is a discrepancy in the aerodynamic behavior of the wing that is presented in Theory of Wing Sections [25] and experimental data by Bezo's [5] for the no-rain condition. Our computed results for the no-rain condition matches well with the results presented in Theory of Wing Sections [25]. The experimental results show that there is an increase in the drag coefficient and decrease in the lift coefficient when the rain intensity increases. A similar behavior is also can be seen from the computed lift and drag coefficients when the rain intensity increases. A similar behavior is also reported in the literature on rain modeling using this benchmark testcase [4,7,9] and our results matches closely with this simulation data. This validated computational model is used for the simulation of rain conditions around the Ahmed body.

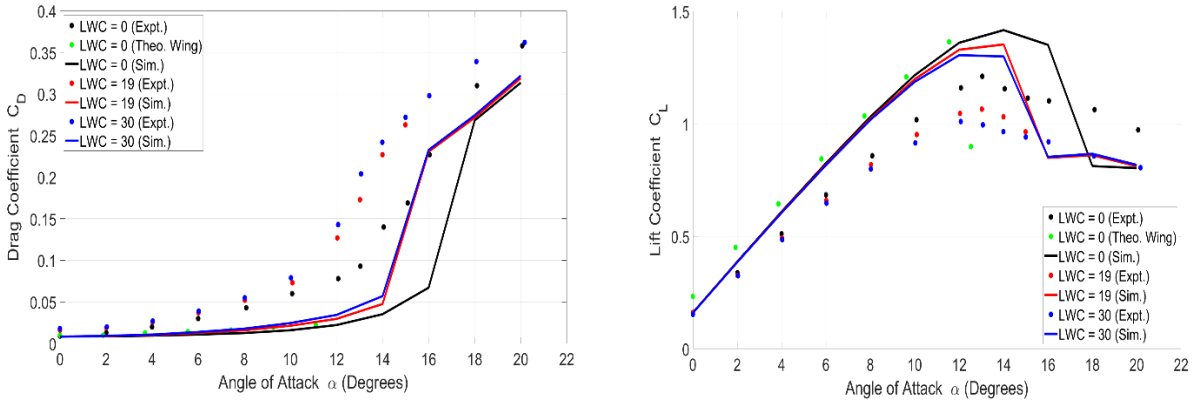

(a) Drag coefficient **(b) Lift coefficient**

Figure 5.2. Comparison of force coefficients from the experimental and numerical results for the NACA64-210 at different rain intensities

B. Validation of the URANS Model

The validation of the URANS model used in these simulations are achieved using the experimental data available for the airflow around the Ahmed body. The geometry of the Ahmed body with the rear slant angles of 25° and 35° and the meshes for the computational simulations are generated using the ANSYS Fluent software. In this geometry, the origin of the coordinate system is placed at front end of Ahmed body, with $x = 0$ start of the model, $y = 0$ at the symmetric plane, and $z = 0$ at the ground plane. The mesh used for the simulation is composed of around 8 million elements for both the slant angles as represented in figure 5.3. As shown in the figure, we have used three different regions for mesh refinement to capture the wake and the flow around the body accurately.

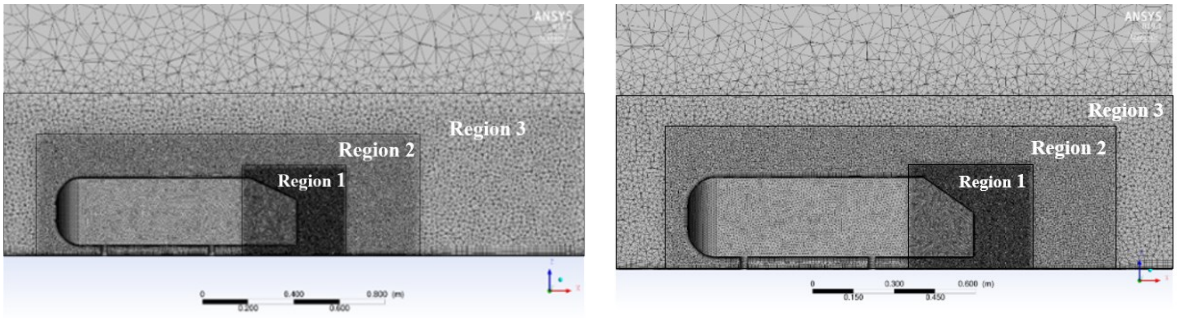

(a) 25 Degree **(b) 35 Degree**

Figure 5.3. Near mesh of the Ahmed body

In these simulations, the velocity inlet is taken as 40 m/s. Since the flow speed less than Mach number 0.3, it is assumed that flow is incompressible, and the density is set to constant value. For the solution of the governing equation, the time derivatives are discretized using first order and the spatial derivatives in the continuity and momentum equations are discretized using a second-order upwind method. A least-squares cell-based method is applied in the estimation of the gradients of the flow variables. A coupled numerical approach is used for the solution of the continuity and the momentum equations. Finally, a first-order upwind technique is applied for the solution of the turbulent kinetic energy and specific dissipation rate equations for the k-ω SST model. The summary of the results from the simulations are tabulated in Table 1. It can be seen from the table that the computational results are in good agreement with the experimental data and results from other simulations.

Table 1: Comparison of the predicted drag coefficient with experimental data and other published data for both slant angles

Slant angle	35°		25°	
	Without stilts	With stilts	Without stilts	With stilts
Experimental data [15]	X	0.260	X	0.285
Our simulation	0.282	0.3096	0.2958	0.3233
Simulation data [19]	0.2895	0.3133	0.3074	X

C. Results from Rain Simulation

The numerical models that are used in Sections A and B are also used for the simulation of wind flow with rain around the Ahmed body. Two different rain intensities, 19 g/m^3 and 30 g/m^3, are used in these simulations to investigate the effect of rain intensities on the aerodynamic forces. We have specified same DPM boundary conditions as the one specified for the NACA64-210 airfoil section.

Table 2 compares the drag coefficient predicted by the numerical rain simulations with the data from the no-rain conditions. We can see a significant effect of rain on the drag coefficients. As expected, it can be seen from the data that the drag coefficient increases as the rain intensity increases. The simulation data shows, for higher rain intensities the drag coefficient is almost three times as compared to the drag coefficient without rain.

Table 2: Comparison of the computed drag coefficients for rain and no-rain conditions for the two slant angles

Rear slant angle		35°		25°	
		Without stilts	With stilts	Without stilts	With stilts
No-rain condition		0.282	0.3096	0.2958	0.3233
Rain conditions	LWC = 19 g/m^3	0.5616	0.5999	0.5909	0.6291
	LWC = 30 g/m^3	0.74	0.7762	0.7472	0.7855

Figure 5.4 shows the profiles of the mean-velocity in the symmetric plane for both rear slant angles. These velocity profiles are compared with the existing experimental data [26] without the rain, and it predicts excellent behavior of the flow in the case of 35°. However, there is a slight variation in the predicted velocity profile as compared with the

experimental data in the case of 25° rear slant angle, but it predicts similar behavior with the numerical simulation data published in [18][19]. The mean velocity profiles with the two-rain intensity i.e., 19 g/m^3 and 30 g/m^3 are also plotted in this figure. It can be seen from the figure that there is a slight variation in velocity profile towards the downstream as the rain intensity increases. However, the change in the velocity profile is insignificant, there is a big difference in the drag coefficient due to the pressure exerted by the impinging rain droplets.

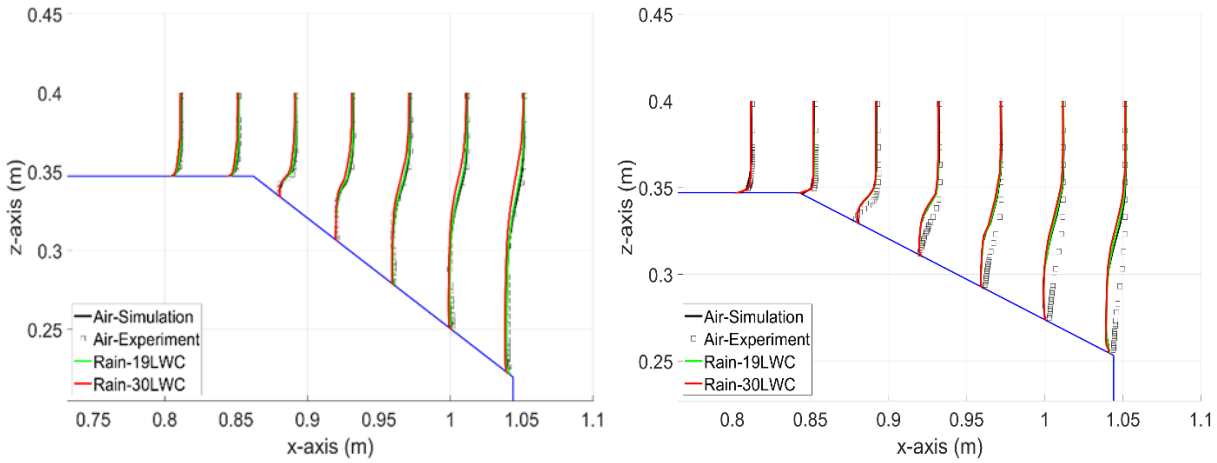

(a) 35 Degree **(b) 25 Degree**

Figure 5.4. Velocity profiles in the symmetric plane

Figures 5.5 and 5.6 compares an oil-film visualization of the experimental data by Lienhart and Becker [26] with the numerical results for rear slant angles of: 35° and 25°, respectively. In this comparison, the Reynolds number is taken as 7.68×10^5 and the fluid medium is taken as air only. These figures show the features of flow observed in the experiments are accurately predicted with the numerical results for both the cases. Figures 5.7 and 5.8 represent an oil-film visualization for both rain intensities and for both rear slant angles. In both these cases, the flow pattern remains the same on the sides and the top for different rain intensities. However, it can be seen from the figures that the separation line moves downstream as the rain intensity increases for both the slant angles.

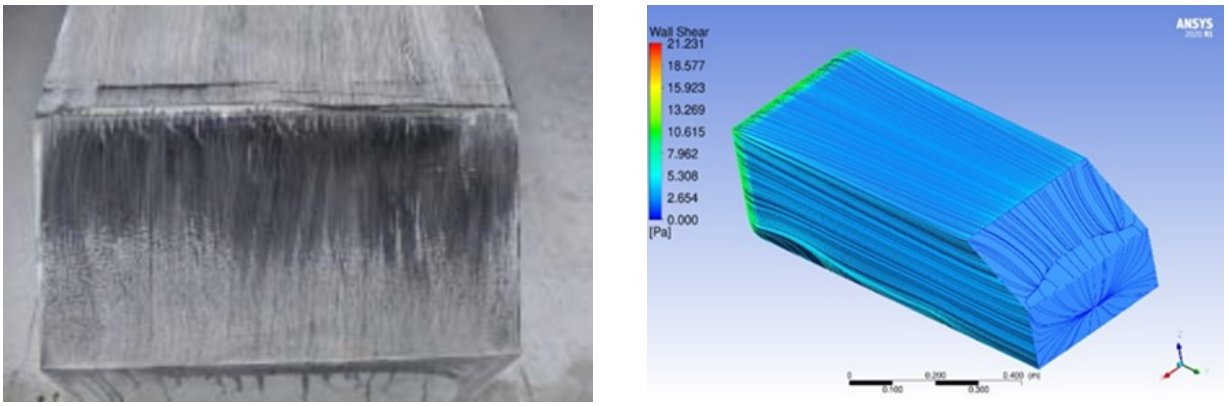

(a) An oil-film visualization by Lienhart and Becker [26] **(b) Numerical results**

Figure 5.5. Comparison of experimental and numerical oil-film visualization at Reynold number 7.68×10^5 for the slant angle of 35°

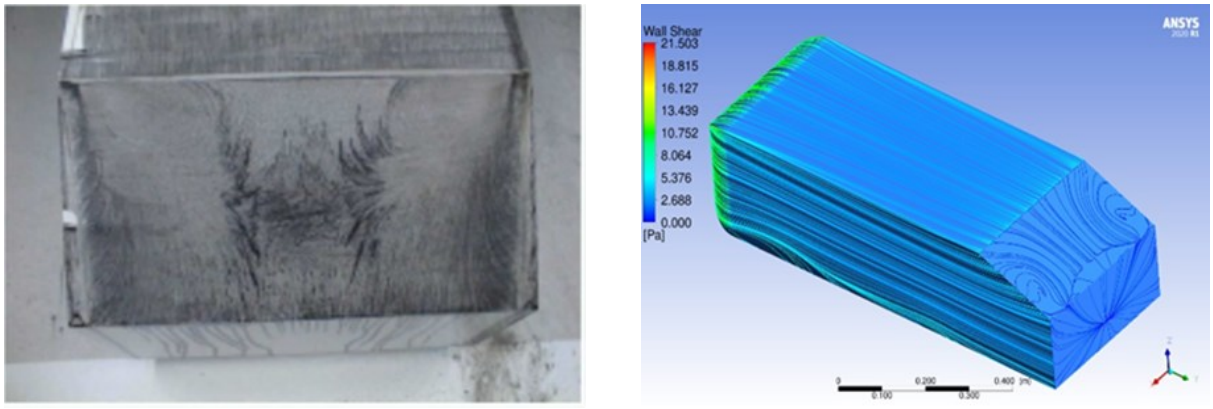

(a) An oil-film visualization by Lienhart and Becker [26] **(b) Numerical results**

Figure 5.6. Comparison of experimental and numerical oil-film visualization at Reynold number 7.68×10^5 for the slant angle of 25°

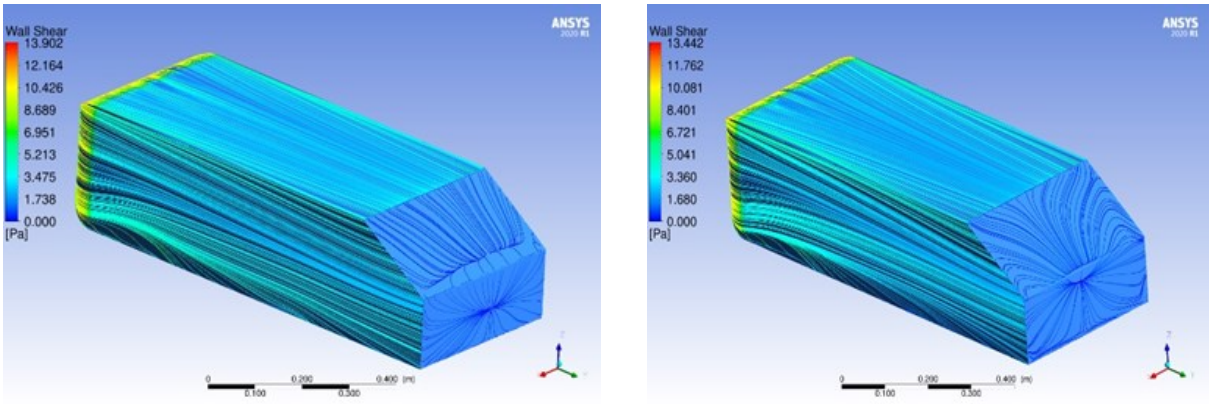

(a) LWC = 19 g/m^3 **(b) LWC = 30 g/m^3**

Figure 5.7. Comparison of oil-film visualizations from the numerical studies for the slant angle of 35°

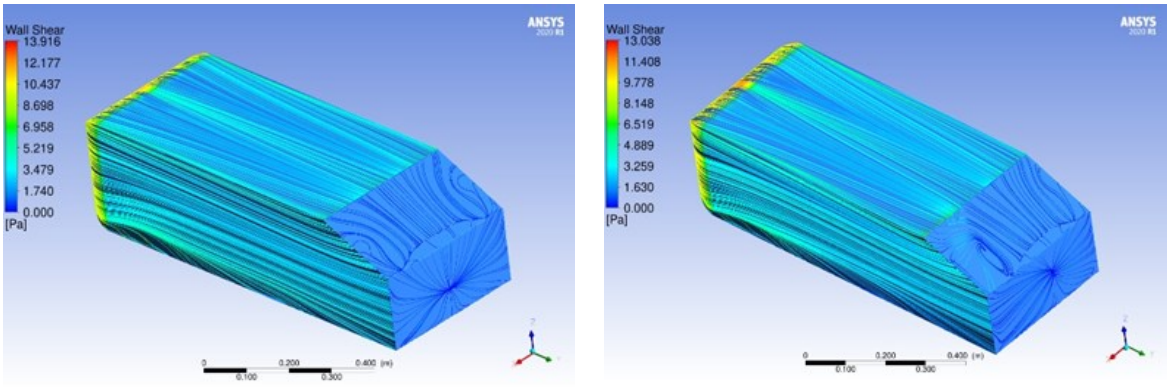

(a) LWC = 19 g/m^3 **(b) LWC = 30 g/m^3**

Figure 5.8. Comparison of oil-film visualizations from the numerical studies for the slant angle of 25°

VI. Conclusions

In this study, we numerically investigated the aerodynamic behavior of the NACA64-210 wing section and the Ahmed body with 25^o and 35^o slant angles, with rain and without rain conditions. A DPM based numerical approach was used for simulating rain and was validated using the experimental data for the NACA64-210 wing section. This validated model was used to study the effect of rain on the aerodynamics performance of the Ahmed body. Numerical simulations with the stilts or without the stilts on which the Ahmed body was supported gave similar results compared to experimental results with a no-rain condition. The simulations showed that the drag force was significantly increased when the Ahmed body is under rain conditions for both rear slant angles. Also, it was observed that the drag coefficient had increased as the rain intensity was increased. The oil-flow visualizations showed that the separation line moved downstream on the slanting surface as the rain intensity was increased. The presented numerical approach can be used for the aerodynamic analysis of an automobile under heavy rain conditions.

Acknowledgments

This research work is supported by NSF award S&AS-1849264. The authors gratefully acknowledge the resources provided by the University of Alabama at Birmingham IT-Research Computing group for high performance computing support (HPC) and CPU time on the Cheaha compute cluster. The authors would like to thank Karthik Remella and John Ibrahim of Ansys, Inc. for their help in setting up the rain model in Ansys/Fluent. The authors also would like to acknowledge Resha Gajera for reviewing and correcting some grammatical errors in this paper.

References

[1] U.S. Department of Transportation, "Freight facts and figures 2015, us department of transportation, bureau of transportation statistics," URL: http://www.princeton.edu/~alaink/Orf467F16/FHWA2015FreightFactsF_complete.pdf.

[2] Rhode, R. V., "Some Effects of Rainfall on Flight of Airplanes and on Instrument Indications," NACA TN903, April 1941.

[3] Benyin L, Cao Y, Wu Z (2017) Numerical Simulation of Aerodynamic Penalties of the DHC-6 Twin Otter Aircraft in Heavy Rain. J Aerosp Eng Mech 1(1):30-39
doi: 10.36959/422/424

[4] Wan, T. and Pan, S.P. Aerodynamic efficiency study under the influence of heavy rain via twophase flow approach, 27th International Congress of the Aeronautical Sciences, 19-24 September, Nice, France, 2010.

[5] Bezos, G. M., & Campbell, B. A. (1993). Development of a large-scale, outdoor, ground-based test capability for evaluating the effect of rain on airfoil lift.

[6] Cao Y, Wu Z, Xu Z (2014) Effects of rainfall on aircraft aerodynamics. Prog Aerosp Sci 71:85–127.
doi:10.1016/j.paerosci.2014.07.003

[7] Hansman, R. J. Jr. and Craig, A. P., "Low Reynolds Number Tests of NACA 64-210, NACA 0012, and Wortmann FS67-K170 Airfoils in Rain," Journal of Aircraft, Vol. 24, No. 8, August 1987.
doi: https://doi.org/10.2514/3.45476

[8] Bezos, G. M., Dunham Jr, R. E., Gentry Jr, G. L., & Melson Jr, W. E. (1992). Wind tunnel aerodynamic characteristics of a transport-type airfoil in a simulated heavy rain environment.

[9] Ismail, M., Yi-hua, C., Ming, Z., & Bakar, A. (2012). Numerical Study of Airfoils Aerodynamic Performance in Heavy Rain Environment.
doi: doi.org/10.5281/zenodo.1332092

[10] Shao, X., Wan, J., Chen, D. et al. Aerodynamic modeling and stability analysis of a high-speed train under strong rain and crosswind conditions. J. Zhejiang Univ. Sci. A 12, 964–970 (2011).
doi: https://doi.org/10.1631/jzus.A11GT001

[11] Harada, N., Kitamura, K., Okutsu, Y., Hamamoto, N., Mori, K., & Nakamura, Y. (2015). Preliminary, One-Way Coupled, Rain-Droplets/Airflow Simulations over Automobile. *International journal of automotive engineering, 6*, 105-112.
doi: https://doi.org/10.20485/jsaeijae.6.4_105

[12] Rahman A, Lownes NE (2012) Analysis of rainfall impacts on platooned vehicle spacing and speed. Transp Res F Traffic Psychol Behav 15(2):395–403
doi: https://doi.org/10.1016/j.trf.2012.03.004

[13] Billot R, El Faouzi NE, De Vuyst F (2009) Multilevel assessment of the impact of rain on drivers' behavior: standardized methodology and empirical analysis. Transportation Research Record: Journal of the Transportation Research Board, No. 2017, pp 134–142
doi: https://doi.org/10.3141/2107-14
[14] Saberi M, Bertini RL (2010) Empirical analysis of the effects of rain on measured freeway traffic parameters. Transportation research board 89th annual meeting. No. 10-2331
[15] S. R. Ahmed, G. Ramm, and G. Faltin. Some salient features of the time averaged ground vehicle wake. SAE Paper 840300, 1984.
doi: https://doi.org/10.4271/840300
[16] Rehan Salahuddin Khan, Sudhakar Umale. CFD Aerodynamic Analysis of Ahmed Body. IJETT – Volume 18 Number 7 – Dec 2014.
doi: 10.14445/22315381/IJETT-V18P262
[17] Hinterberger, C., M. García-Villalba, W. Rodi (2004) Large eddy simulation of flow around the Ahmed body. In: McCallen R, Browand F, Ross J (Eds.) Lecture notes in applied and computational mechanics / The aerodynamics of heavy vehicles: trucks, busses, and trains, Springer Verlag.
doi: https://doi.org/10.1007/978-3-540-44419-0_7
[18] E. Guilmineau ∗, G.B. Deng, A. Leroyer, P. Queutey, M. Visonneau, J. Wackers. Assessment of hybrid RANS-LES formulations for flow simulation around the Ahmed body. Computers and Fluids 176 (2018) 302–319.
doi: https://doi.org/10.1016/j.compfluid.2017.01.005
[19] E Guilmineau. Computational study of flow around a simplified car body. J Wind Eng Ind Aerodyn 2008;96(6):1207–17.
doi: https://doi.org/10.1016/j.jweia.2007.06.041
[20] Laboratoire de Me´canique des Fluides, CNRS UMR 6598, Ecole Centrale de Nantes, 44321 Nantes Cedex 3, France. Computational study of flow around a simplified car body. Journal of Wind Engineering and Industrial Aerodynamics 96 (2008) 1207–1217.
[21] Markowitz, A. M., "Raindrop Size Distribution Expression," Journal of Applied Meteorology, Vol. 15, 1976, pp. 1029-1031. URL: http://www.jstor.org/stable/26177317.
[22] ANSYS Fluent Theory Guide, 2020R1, January 2020.
[23] S. Niu, X. Jia, J. Sang, X. Liu, C. Lu, and Y. Liu, "Distributions of raindrop sizes and fall velocities in a semiarid plateau climate: convective versus stratiform rains," Journal of Applied Meteorology and Climatology, vol. 49, no. 4, pp. 632–645, 2010.
doi: https://doi.org/10.1175/2009JAMC2208.1
[24] Tokay, A., A. Kruger, and W. Krajewski, Comparison of drop-size distribution measurements by impact and optical disdrometers, J. Appl. Meteorol., 40, 2083– 2097, 2001.
doi: https://doi.org/10.1175/1520-0450(2001)040<2083:CODSDM>2.0.CO;2
[25] Abbot, I. H. and von Doenhoff, A. E., Theory of Wing Section: Including a Summary of Airfoil Data, Dover Publication, New York, 1959.
[26] H. Lienhart and S. Becker. Flow and turbulence structure in the wake of a simplified car model. SAE Paper 2003-01-0656, 2003.
doi: https://doi.org/10.1007/978-3-540-45466-3_39